Structure-Based Design of a Highly Active Vitamin D Hydroxylase from *Streptomyces griseolus* CYP105A1[†,‡]

Keiko Hayashi,[§] Hiroshi Sugimoto,*[,||] Raku Shinkyo,[⊥] Masato Yamada,[§] Shinnosuke Ikeda,[§] Shinichi Ikushiro,[§] Masaki Kamakura,[§] Yoshitsugu Shiro,[||] and Toshiyuki Sakaki*[,§]

Department of Biotechnology, Faculty of Engineering, Toyama Prefectural University, 5180 Kurokawa, Imizu, Toyama 939-0398, Japan, RIKEN SPring-8 Center, Harima Institute, Sayo, Hyogo 679-5148, Japan, and Division of Food Science and Biotechnology, Graduate School of Agriculture, Kyoto University, Sakyo-ku, Kyoto 606-8502, Japan

Received June 29, 2008; Revised Manuscript Received August 19, 2008

ABSTRACT: CYP105A1 from *Streptomyces griseolus* has the capability of converting vitamin D_3 (VD_3) to its active form, 1α,25-dihydroxyvitamin D_3 (1α,25$(OH)_2D_3$) by a two-step hydroxylation reaction. Our previous structural study has suggested that Arg73 and Arg84 are key residues for the activities of CYP105A1. In this study, we prepared a series of single and double mutants by site-directed mutagenesis focusing on these two residues of CYP105A1 to obtain the hyperactive vitamin D_3 hydroxylase. R84F mutation altered the substrate specificity that gives preference to the 1α-hydroxylation of 25-hydroxyvitamin D_3 over the 25-hydroxylation of 1α-hydroxyvitamin D_3, opposite to the wild type and other mutants. The double mutant R73V/R84A exhibited 435- and 110-fold higher k_{cat}/K_m values for the 25-hydroxylation of 1α-hydroxyvitamin D_3 and 1α-hydroxylation of 25-hydroxyvitamin D_3, respectively, compared with the wild-type enzyme. These values notably exceed those of CYP27A1, which is the physiologically essential VD_3 hydroxylase. Thus, we successfully generated useful enzymes of altered substrate preference and hyperactivity. Structural and kinetic analyses of single and double mutants suggest that the amino acid residues at positions 73 and 84 affect the location and conformation of the bound compound in the reaction site and those in the transient binding site, respectively.

Vitamin D_3 (VD_3)[1] is produced from 7-dehydrocholesterol in the skin upon exposure to sunlight. It has no hormonal activity itself, but the dihydroxylated metabolite, 1α,25-dihydroxyvitamin D_3 (1α,25$(OH)_2D_3$), is hormonally active, mediating its biological effects by binding to the vitamin D receptor (VDR). Activation of the VDR in the intestine, bone, kidney, and parathyroid gland maintains calcium and phosphorus concentrations in the blood and preserves bone mineral content. The hydroxylation of VD_3 is catalyzed in two steps by CYP enzymes in humans and other mammals. The first step is the hydroxylation of the C25 position of VD_3 to produce 25$(OH)D_3$ (25-pathway in Figure 1) by mitochondrial CYP27A1 or microsomal CYP2R1 in the liver. The second reaction is the hydroxylation of the C1α-position catalyzed by mitochondrial CYP27B1 in the kidneys to produce 1α,25$(OH)_2D_3$ from 25$(OH)D_3$. Another mitochondrial enzyme, CYP24A1, metabolizes 1α,25$(OH)_2D_3$ by sequential monooxygenation to regulate the serum level of 1α,25$(OH)_2D_3$ (*1*).

The industrial production of 1α,25$(OH)_2D_3$ from VD_3 uses a bioconversion system of *Amycolata autotrophica*, which is one of the successful applications of the P450 reaction on the industrial scale (*2, 3*). The primary structure of the cloned gene indicated that the 25-hydroxylase of vitamin D_3 is a water-soluble P450 named CYP105A2 (*4*). We found that *Streptomyces griseolus* CYP105A1 also has weak activities of both 25-hydroxylation and 1α-hydroxylation of vitamin D_3 to produce 1α,25$(OH)_2D_3$ (*5*). Originally, this CYP was cloned by Omer et al. (*6*) as a sulfonylurea herbicide-metabolizing enzyme, P450SU-1, which shows a 55% identity of amino acid sequence with CYP105A2. Recent crystal structure analysis of CYP105A1 revealed that the substrate-binding pocket of CYP105A1 contains three arginine residues (Arg73, Arg84, and Arg193) (Figure 2). The Ala-scan mutation analysis suggested that these residues play key roles in substrate recognition (*7, 8*). Substitution of Arg193 to Ala (R193A) significantly reduced the activity. The crystal structure in the complex with 1α,25$(OH)_2D_3$ strongly suggests that a side chain of Arg193 interacts with the 3β-OH group of the substrate. In contrast, R73A and R84A showed much higher activity than the wild type, suggesting that Arg73 and Arg84 residues have an inhibitory effect on the activity.

[†] This work was supported in part by the Ministry of Education, Culture, Sports, Science and Technology grant (to H.S. and Y.S.) and the Novozyme Japan Research Fund (to T.S.).

[‡] The atomic coordinates and structure factors (PDB codes 3CV8 and 3CV9) have been deposited in the Protein Data Bank, Research Collaboratory for Structural Bioinformatics, Rutgers University, New Brunswick, NJ (http://www.rcsb.org/).

* To whom correspondence should be addressed. H.S.: phone, +81-791-58-2817; fax, +81-791-58-2818; e-mail, sugimoto@spring8.or.jp. T.S.: phone, +81-766-56-7500; fax, +81-766-56-2498; e-mail, tsakaki@pu-toyama.ac.jp.

[§] Toyama Prefectural University.

[||] RIKEN Spring-8 Center.

[⊥] Kyoto University.

[1] Abbreviations: CYP, cytochrome P450; VD_3, vitamin D_3; 25$(OH)D_3$, 25-hydroxyvitamin D_3; 1α$(OH)D_3$, 1α-hydroxyvitamin D_3; 1α,25$(OH)_2D_3$, 1α,25-dihydroxyvitamin D_3; rmsd, root mean square deviation.

10.1021/bi801222d CCC: $40.75
Published on Web 10/21/2008

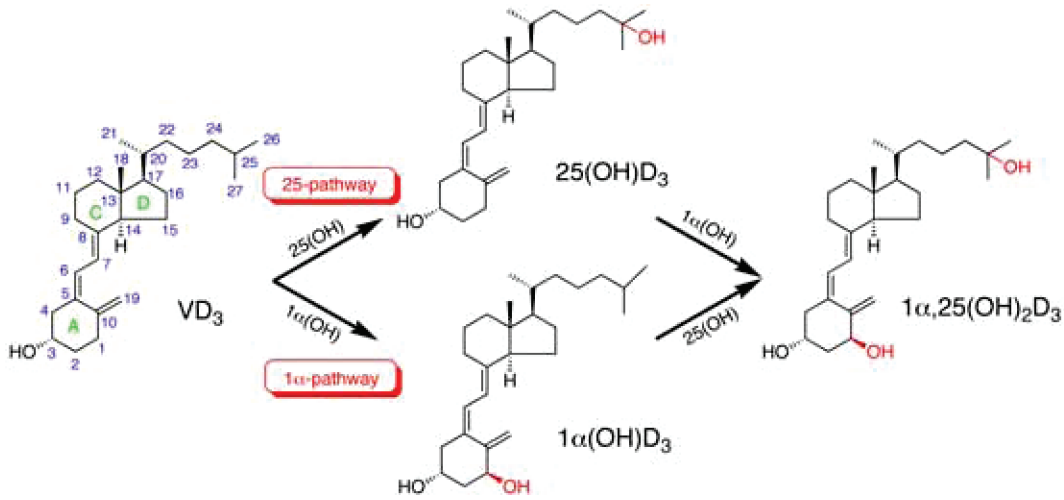

FIGURE 1: Metabolic pathways of vitamin D_3 by the wild type and mutants of CYP105A1.

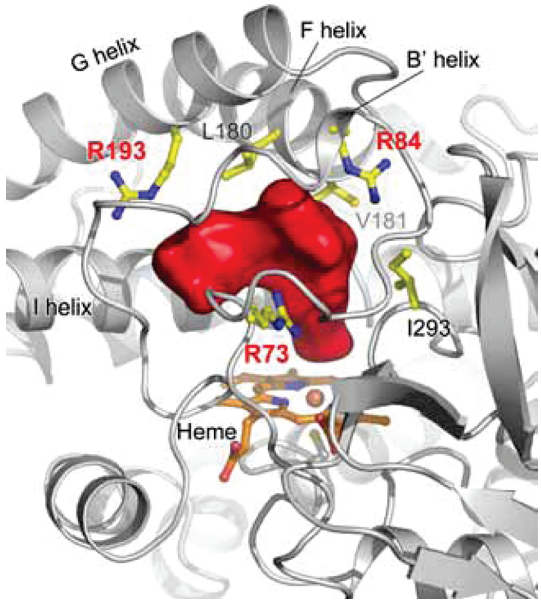

FIGURE 2: Active site of wild-type CYP105A1 contains three Arg residues (R73, R84, and R193). The substrate-binding cavity is represented as a red surface. Atoms for the disordered region in the B′ helix are tentatively modeled using the R84A mutant as a guide.

In this report, we made a further attempt to enhance the vitamin D hydroxylation activity of CYP105A1 by mutating two Arg residues into various amino acids. Characterization of the enzymatic parameters revealed that one of those mutants exhibits 400-fold higher activity compared with the wild type. A unique mutant that prefers 1α-hydroxylation to 25-hydroxylation was also generated.

MATERIALS AND METHODS

Materials. DNA modifying enzymes and restriction enzymes were purchased from Takara Shuzo Co. Ltd. (Kyoto, Japan). *Escherichia coli* JM109 (Takara Shuzo Co.) was used as a host strain. Ferredoxin and NADPH−ferredoxin reductase from spinach were purchased from Sigma (St. Louis, MO). Vitamin D_3, 1α(OH)D_3, 1α,25(OH)$_2D_3$, glucose dehydrogenase, and catalase were purchased from Wako Pure Chemical Industries, Ltd. (Osaka, Japan). 25(OH)D_3 was purchased from Funakoshi Co. Ltd. (Tokyo, Japan). *Streptomyces griseolus* CYP105A1 and ferredoxin genes were kindly provided by Sumitomo Chemical Co. Ltd. (Takarazuka, Japan). NADPH was purchased from Oriental Yeast Co. Ltd. (Tokyo, Japan). Other chemicals used were of the highest quality commercially available.

Table 1: Oligonucleotides Used To Generate CYP105A1 Mutants[a]

mutation	oligonucleotides
R73A	5′-CGGCTGTCCTCCAACGCCGACGGACGACAAC-3′
	5′-GTTGTCGTCCGTCGCGTTGGAGGACAGCCG-3′
R73V	5′-CGGCTGTCCTCCAACGTCACGGACGACAAC-3′
	5′-GTTGTCGTCCGTGACGTTGGAGGACAGCCG-3′
R73L	5′-CGGCTGTCCTCCAACCTCACGGACGACAAC-3′
	5′-GTTGTCGTCCGTGAGGTTGGAGGACAGCCG-3′
R73F	5′-CGGCTGTCCTCCAACTTCACGGACGACAAC-3′
	5′-GTTGTCGTCCGTGAAGTTGGAGGACAGCCG-3′
R84A	5′-CCGCCACGTCACCGGCCTTCGAGGCCGTCC-3′
	5′-GGACGGCCTCGAAGGCCGGTGACGTGGCGG-3′
R84V	5′-CCGCCACGTCACCGGTCTTCGAGGCCGTCC-3′
	5′-GGACGGCCTCGAAGACCGGTGACGTGGCGG-3′
R84L	5′-CCGCCACGTCACCGCTCTTCGAGGCCGTCC-3′
	5′-GGACGGCCTCGAAGAGCGGTGACGTGGCGG-3′
R84Q	5′-CCGCCACGTCACCGCAATTCGAGGCCGTCC-3′
	5′-GGACGGCCTCGAATTGCGGTGACGTGGCGG-3′
R84F	5′-CCGCCACGTCACCGTTCTTCGAGGCCGTCC-3′
	5′-GGACGGCCTCGAAGAACGGTGACGTGGCGG-3′

[a] The mutated nucleotides are underlined.

Construction of Expression Plasmids for Wild Type and Mutants of CYP105A1. Mutants were generated by the QuickChange site-directed mutagenesis kit (Stratagene) according to the instruction manual. The oligonucleotide primers for mutagenesis are shown in Table 1. Corrected generation of desired mutations was confirmed by DNA sequencing. The expression plasmids for wild type and mutants of CYP105A1 with the His tag were constructed as described previously (*9*). Each of the resultant expression plasmids was introduced into *E. coli* JM109 cells.

Expression of Wild Type and Mutants of CYP105A1 in E. coli Cells. Recombinant *E. coli* cells were grown in TB medium containing 50 μg/mL ampicillin at 37 °C as described previously (*9*). The induction of transcription of CYP105A1 was initiated by addition of isopropyl thio-β-D-galactpyranoside (IPTG) at a final concentration of 1 mM when the cell density (OD_{660}) reached 0.5. δ-Aminolevulinic acid was also added at a final concentration of 0.5 mM. The recombinant *E. coli* cells were shaken at 23 °C for 46 h.

Purification of Wild Type and Mutants of CYP105A1. The cytosolic fraction prepared from each of the recombinant *E. coli* cells was applied to Ni Sepharose (Bio-Rad Profinity IMAC Resins) equilibrated with 20 mM Tris-HCl buffer (pH 7.4) at a flow rate of 1 mL/min. After adsorption of wild type or mutant CYP105A1, the column was washed with 10 column volumes of the same buffer and eluted with a linear gradient of 0−120 mM imidazole in 20 mM Tris-HCl buffer (pH 7.4). The eluted wild type or mutant CYP105A1 was applied to a hydroxylapatite column (Econo-Pack HTC-II; Bio-Rad, Hercules, CA) equilibrated with 10 mM potassium phosphate (pH 7.4). The wild type or mutant CYP105A1 that passed through from hydroxylapatite column was applied to a Mono Q 5/50 GL column (GE Healthcare) equilibrated with 20 mM Tris-HCl buffer (pH 7.4). After adsorption of wild type or mutant CYP105A1, the column was eluted with a linear gradient of 50−600 mM NaCl in 20 mM Tris-HCl buffer (pH 7.4).

Spectral Analysis. The reduced CO difference spectra of wild type or mutant CYP105A1 was measured with a Hitachi U-3310 spectrophotometer with a head-on photomultiplier (Tokyo, Japan). The P450 content of the purified wild type or mutant CYP105A1 was estimated using a molar extinction coefficient of 110 mM^{-1} cm^{-1} at 417 nm (*9*).

Measurement of the Activity. Each of the hydroxylation activities with vitamin D_3, 1α(OH)D_3, or 25(OH)D_3 as a substrate was measured in the reconstituted system containing 0.2 μM enzyme, 0.1 mg/mL spinach ferredoxin, 0.1 unit/mL spinach ferredoxin reductase, 1 unit/mL glucose dehydrogenase, 1% glucose, 0.1 mg/mL catalase, 1 mM NADPH, 0.5−10.0 μM substrate, 100 mM Tris-HCl (pH 7.4), and 1 mM EDTA at 30 °C. The substrates were dissolved in ethanol and added to the reaction mixture. The final concentration of ethanol in the reaction mixture was 1%. The kinetic parameters K_m and k_{cat} were calculated by the nonlinear regression analysis using the Kaleida-Graph (Synergy software). On the other hand, the reaction mixture containing 0.8 μM enzyme was used to observe a two-step hydroxylation of VD_3. Aliquots of the reaction mixture were collected after varying time intervals and extracted with 4 volumes of chloroform−methanol (3:1). The organic phase was recovered and dried. The resulting residue was solubilized with acetonitrile and applied to HPLC under the following conditions: column, YMC-Pack ODS-AM (4.6 × 300 mm) (YMC Co., Tokyo, Japan); UV detection, 265 nm; flow rate, 1.0 mL/min; column temperature, 40 °C; mobile phase, a linear gradient of 70−100% acetonitrile aqueous solution per 15 min followed by 100% acetonitrile for 25 min for the analysis of the metabolites.

Crystallization and Structure Refinement. The R84F mutant was crystallized in the reservoir condition of 16% PEGMME2000, 10% 2-methyl-2,4-pentanediol (MPD), 0.1 M Bis-Tris (pH 6.1), and 0.2 M NaCl using the same protocol as previously described (*5*). For the preparation of R73A/R84A−product complex, 1α,25(OH)$_2$$D_3$ was dissolved at 6 mM in 60% ethanol and added to the purified protein (0.03 mM) in a 10-fold molar excess. The complex was kept on ice for 1 day and then concentrated to 0.3 mM. The R73A/R84A mutant was crystallized in reservoir solution composed of 26% PEGMME2000, 0.1 M Bis-Tris (pH 6.2), and 0.2 M NaCl. All crystals have similar unit cell dimensions and molecular packing compared with the wild type enzyme (*9*).

Table 2: Statistics of X-ray Data Collection and Structure Refinement

	R84F	R73A/R84A-1α,25(OH)$_2$$D_3$
PDB code	3CV8	3CV9
resolution (Å)	20−2.0	20−1.7
high-resolution shell	2.07−2.00	1.76−1.70
space group	$P2_12_12_1$	$P2_12_12_1$
unit cell dimensions (Å)	a = 52.5, b = 53.4, c = 139.0	a = 53.3, b = 53.7, c = 140.6
wavelength (Å)	1.0	1.0
observed reflections	144358	319092
unique reflections	27037	45139
R_{merge} (%)[a,b]	7.3 (19.1)	4.0 (33.7)
completeness (%)[a]	99.4 (98.2)	98.5 (87.1)
$I/\sigma(I)$[a]	23.1 (8.3)	28.8 (5.1)
redundancy[a]	5.3 (5.4)	7.1 (5.3)
R_{work}/R_{free}[c]	0.181/ 0.230	0.199/0.253
no. of atoms	3496	3686
average B values (Å^2)		
protein	17.5	21.8
waters	26.8	32.6
other entities	9.7	18.4
rmsd bond (Å)	0.011	0.014
rmsd angle (deg)	1.27	1.55

[a] Numbers in parentheses refer to the highest resolution shell. [b] $R_{merge} = \sum_{hkl}\sum_i|I_i(hkl) - \langle I(hkl)\rangle|/\sum_{hkl}\sum_i I_i(hkl)$, where $\langle I(hkl)\rangle$ is the average intensity of the i observations. [c] $R_{work} = \sum_{hkl}|F_o(hkl)| - |F_c(hkl)|/\sum_{hkl}|F_o(hkl)|$. R_{work} is calculated for 95% of reflections used for structure refinement. R_{free} is calculated for the remaining 5% of reflections randomly selected and excluded from refinement.

The crystals were cryoprotected by transferring to the buffer consisting of the reservoir solution and an additional 25% glycerol. X-ray diffraction data were collected using a Quantum 210 CCD detector (ADSC) on BL44B2 at SPring-8, Japan. All data were integrated and scaled using the HKL2000 program (*10*). The structure of R84A (PDB code 2ZBZ) was used as the starting model for the refinement. The model of the wild type enzyme was placed directly into the unit cell of the mutant and subjected to rigid body refinement and restrained refinement using REFMAC5 (*11*). The model was further refined with multiple rounds of manual rebuilding using Coot (*12*) followed by the restrained refinement. Data collection and refinement statistics are shown in Table 2.

Other Methods. The concentrations of vitamin D_3 derivatives were estimated by their molar extinction coefficient of 1.80×10^4 M^{-1} cm^{-1} at 264 nm (*13*). Docking experiments were performed by previously described procedures (*9*) using Autodock 4 (*14*). All figures of protein structure are prepared using PyMol software (http://www.pymol.org). The cavity in Figure 2 was calculated by VOIDOO program using the probe radius 1.4 Å (*15*) and protocol described in http://xray.bmc.uu.se/usf/vis_tunnel.html. The least-squares superposition calculations for atomic models were performed by LSQKAB program (*11*).

RESULTS AND DISCUSSION

Expression, Purification, Spectral Properties, and Activities of Wild Type and Mutants of CYP105A1. The crystal structure of CYP105A1 has suggested that Arg73, Arg84, Val88, Leu180, Val181, Arg193, Ser236, Ile243, and ILe293 comprise the substrate-binding site (*9*). We scanned these residues by substitution to Ala in the previous structural analysis. Of these mutants, V88A, L180A, V180A, R193A, and I243A showed significantly low or undetectable activity

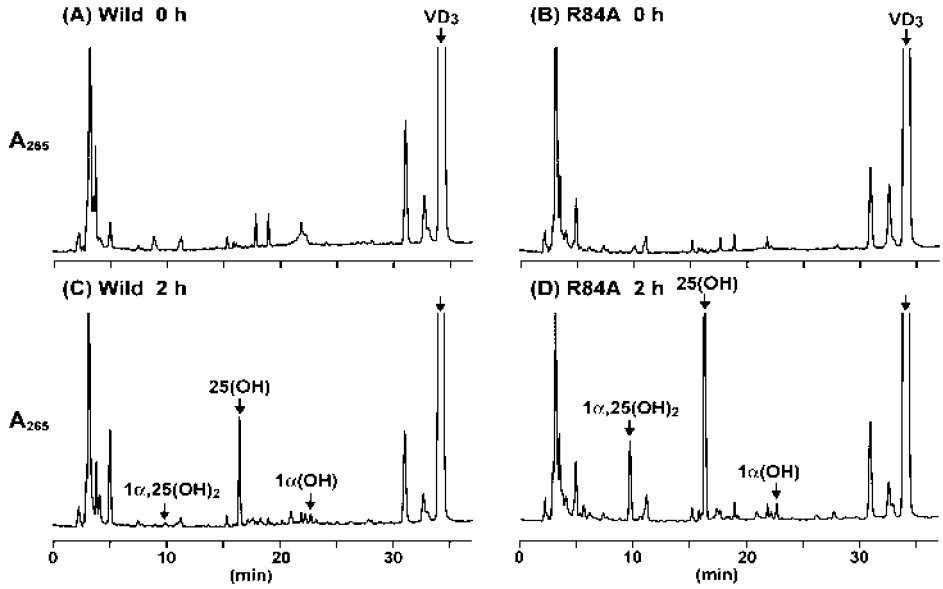

FIGURE 3: HPLC profiles of vitamin D and its metabolites formed by wild type of CYP105A1 (A and C) and its mutant R84A (B and D). After incubation with 10 μM vitamin D_3 for 0 (A and B) or 2 h (C and D), the reaction mixture was extracted and analyzed by HPLC as described under Materials and Methods.

(*9*), while R73A and R84A showed remarkably higher activities in the 25-hydroxylation and the 1α-hydroxylation than the wild type enzyme. From this point, we prepared a series of the single and double mutants of these residues (Arg73 and Arg84) and examined their enzymatic properties.

The mutants of CYP105A1 we prepared in this study were expressed in the 1000−5000 nmol/L culture, similarly to the wild type enzyme, and were purified according to the procedure described elsewhere. All the enzymes thus purified were stable enough at room temperature for measurements of their activities and absorption spectra and for crystallization. As for the wild type enzyme, the mutants showed optical absorption spectra with a Soret maximum at 417 nm, indicating that the heme iron is in the ferric low spin state. These observations suggested that the mutation we introduced at the position(s) of Arg73 and/or Arg84 in CYP105A1 did not seriously disturb the active site structure. It is noted that all of crystal structures of the wild type and mutants of CYP105A1 with and without 1α,25$(OH)_2D_3$ had no water molecule coordinated to heme iron. We assume that exposure to X-ray may reduce heme iron as in the case of CYP2R1 (*16*).

In the metabolism of VD_3, 1α$(OH)D_3$, and 25$(OH)D_3$ by the wild type of CYP105A1, the dual metabolic pathways have been demonstrated, as shown in Figure 1. One is a conversion of VD_3 to 25$(OH)D_3$ and then to 1α,25$(OH)_2D_3$ (25-pathway), while the other one is a pathway via 1α$(OH)D_3$ as an intermediate (1α-pathway). In the HPLC profiles of the VD_3 hydroxylation by wild type CYP105A1 (Figure 3A,C), the amount of 25$(OH)D_3$ is predominant as the product of this reaction, while very small amounts of 1α$(OH)D_3$ and 1α,25$(OH)_2D_3$ are obtained, suggesting that the major pathway is the 25-pathway. Upon the mutation of the targeted residues of CYP105A1, the HPLC profiles of the metabolites (amounts and ratio) were dramatically altered, as shown for the R84A mutant (Figure 3B,D). Detailed analysis of the HPLC profiles to obtain their kinetic parameters (Tables 3 and 4) could evaluate the mutational effect of Arg73 and Arg84 on the enzymatic activities and specificities of CYP105A1 in the VD_3 activation.

Table 3: Kinetic Parameters of Wild Type and Mutants of CYP105A1 for 25-Hydroxylation of 1α$(OH)D_3$ and 1α-Hydroxylation of 25$(OH)D_3$

CYP105A1	substrate	K_m (μM)	k_{cat} (min^{-1})	k_{cat}/K_m	relative k_{cat}/K_m[a]
wild type	1α(OH)	10.1 ± 1.8	0.0076 ± 0.0002	0.00075	1
	25(OH)	4.4 ± 1.3	0.0026 ± 0.0003	0.00059	1
R84A	1α(OH)	8.7 ± 0.2	0.253 ± 0.005	0.029	39
	25(OH)	2.4 ± 0.4	0.025 ± 0.001	0.010	17
R84V	1α(OH)	7.6 ± 3.5	0.125 ± 0.029	0.017	23
	25(OH)	1.8 ± 1.6	0.014 ± 0.001	0.008	14
R84L	1α(OH)	1.9 ± 0.1	0.023 ± 0.001	0.012	16
	25(OH)	2.9 ± 0.8	0.015 ± 0.001	0.005	8
R84F	1α(OH)	6.4 ± 2.8	0.039 ± 0.004	0.006	8
	25(OH)	1.0 ± 0.2	0.025 ± 0.001	0.025	43
R84Q	1α(OH)	14.2 ± 0.6	0.122 ± 0.007	0.009	12
	25(OH)	3.6 ± 2.0	0.011 ± 0.003	0.003	5
R73A	1α(OH)	7.1 ± 2.1	0.089 ± 0.005	0.013	17
	25(OH)	3.6 ± 1.4	0.020 ± 0.001	0.005	8
R73V	1α(OH)	17.9 ± 3.7	0.371 ± 0.056	0.021	28
	25(OH)	2.7 ± 0.4	0.025 ± 0.001	0.009	15
R73L	1α(OH)	11.2 ± 6.1	0.256 ± 0.080	0.023	31
	25(OH)	3.5 ± 0.4	0.041 ± 0.003	0.012	20
R73F	1α(OH)	4.7 ± 0.7	0.021 ± 0.001	0.004	5
	25(OH)	1.5 ± 0.1	0.0025 ± 0.0001	0.002	3

[a] The values are relative to the k_{cat}/K_m value of the wild type.

Enzymatic Properties of Arg84 Mutants. As shown in Table 3, we prepared the Arg84 mutants (R84Q, R84A, R84V, R84L, and R84F) and obtained the kinetic parameters (K_m, k_{cat}, and k_{cat}/K_m) of the 25-hydroxylation reaction of the 1α$(OH)VD_3$ (the second reaction of the 1α-pathway) and of the 1α-hydroxylation reaction of the 25$(OH)VD_3$ (the second reaction of the 25-pathway). The former reaction mimics the reaction of CYP27A1, and the latter does that of CYP27B1, both of which are natural VD_3 hydroxylases in mammals.

In the 25-hydroxylation of 1α$(OH)D_3$, all the mutants show k_{cat} and k_{cat}/K_m values much higher than the wild type. Of these mutants, R84A gives the highest k_{cat}/K_m value in this reaction, which is more than 30 times higher than the wild type enzyme. In the previous crystallographic study of

the wild type and R84A mutant, it was found that substitution of Arg84 in the first turn of B′ helix (Figure 2) to Ala did not affect the overall tertiary structure of CYP105A1, but the slightly open structure of the F helix is induced by loss of the interaction between the Arg84 side chain and the O on Ser183 (F/G loop). Since the K_m values of wild-type and R84A mutant are comparable (Table 3), it has been suggested that some change in the gating mechanism affects the adaptability of the hydrophobic residues of the F helix (Leu180 and Val181) for substrate recognition during the hydroxylation of substrates by the ferryl oxygen, eventually enhancing the enzymatic activity.

As the results in Table 3 show, k_{cat}/K_m values of four types of Arg84 mutant in the 25-hydroxylation are in the order of R84A > R84V > R84L > R84F, demonstrating that the hydrophobicity and the volume of the side chain at position 84 are critical for the activity.

On the other hand, concerning the 1α-hydroxylation of 25(OH)D_3, the R84F mutant exhibits the highest activity among all of the Arg84 mutants. This character is substantially contributed by a significantly high k_{cat} and a remarkably low K_m value for the 1α-hydroxylation of 25(OH)D_3, showing its high catalytic activity and a high affinity for 25(OH)D_3 of the R84F mutants of CYP105A1. The k_{cat}/K_m value for the 1α-hydroxylation of 25(OH)D_3 was increased by 43 times upon the R84F mutation. As a result, it is also notable that the k_{cat}/K_m values of the 1α-hydroxylation of 25(OH)D_3 are larger than those of the 25-hydroxylation of 1α(OH)D_3; that is, the ratios of the 1α-hydroxylation to the 25-hydroxylation are 4.2 for the R84F mutants, in sharp contrast to 0.3−0.8 for the wild type and other mutants. Thus, the altered specificity of the R84F mutant mimics CYP27B1, which is a mammalian VD_3 1α-hydroxylase (*17*).

Previous studies on other CYPs suggest that the B′ and F helices are important for the control of substrate specificity (*18*). The above difference in enzymatic properties between R84A and R84F appears to be attributable to conformational differences of the substrate-access channel and substrate-binding pocket. In the present crystal structural analysis of the R84F mutant in noncomplex form, it was found that the position of the B′ helix and the shape of the substrate binding pocket are significantly affected by the mutation compared with the wild type and R84A mutant (Figure 4). The room for 1α,25(OH)$_2D_3$ binding that has been observed in the R84A mutant is mostly occupied by the side chain of F84 in the B′ helix because the more ordered B′ helix shifts to tightly pack with the F helix, which may be the reason our attempt to cocrystallize the R84F mutant with 1α,25(OH)$_2D_3$ was unsuccessful. Although the precise mode of substrate binding in CYP105A1 is not yet known, the location of the F84 side chain may indicate the direct interaction to increase the binding affinity of 25(OH)D_3 based on its low K_m value (Table 3). The conformations of other potential substrate-binding regions are also affected by the R84F mutation (Figure 4). Note that residues L180 and V181 in the F helix contact F84 by hydrophobic interaction. In addition, I293-A294 of the loop region after the K helix is also affected and creates the space for binding of the compound. Thus, R84F bears the pocket structure that more resembles that of the R84A mutant in the complex with 1α,25(OH)$_2D_3$, rather than R84A in noncomplex form. These observations suggest

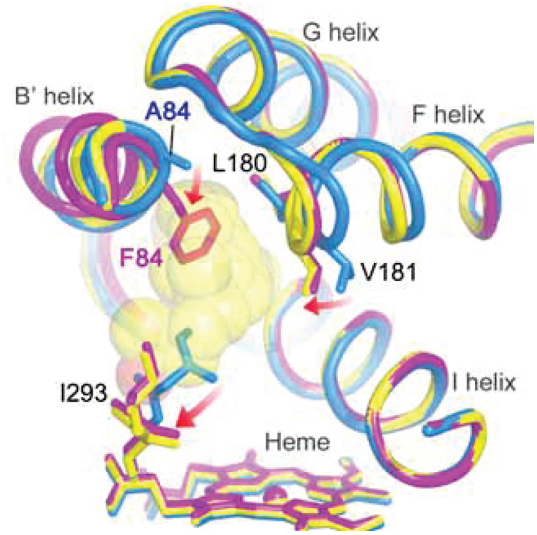

FIGURE 4: Comparison of tertiary structures of the free form of R84F (purple), free form of R84A (cyan), and R84A in complex with 1α,25(OH)$_2D_3$ (yellow). The bound 1α,25(OH)$_2D_3$ into R84A is represented by the transparent spheres. Structural difference between R84F and R84A is indicated as red arrows.

Table 4: Kinetic Parameters of Double Mutants of CYP105A1 for 25-Hydroxylation of 1α(OH)D_3, 1α-Hydroxylation of 25(OH)D_3, and 25-Hydroxylation of Vitamin D_3

CYP105A1	substrate	K_m (μM)	k_{cat} (min^{-1})	k_{cat}/K_m	relative k_{cat}/K_m[a]
R73A/R84A	1α(OH)	9.0 ± 0.8	2.15 ± 0.13	0.239	319
	25(OH)	1.1 ± 0.1	0.071 ± 0.020	0.065	110
	VD_3	1.6 ± 0.1	0.063 ± 0.002	0.039	
R73V/R84A	1α(OH)	6.5 ± 0.4	2.12 ± 0.12	0.326	435
	25(OH)	2.2 ± 0.1	0.136 ± 0.004	0.062	105
	VD_3	3.5 ± 0.1	0.141 ± 0.001	0.040	
R73V/R84F	1α(OH)	5.3 ± 0.7	1.44 ± 0.02	0.272	363
	25(OH)	1.6 ± 0.1	0.047 ± 0.001	0.029	49
	VD_3	3.0 ± 0.4	0.097 ± 0.006	0.032	

[a] The values are relative to the k_{cat}/K_m value of the wild type in Table 3.

that the conformational changes within the active site pocket in the wide area result in the unique enzymatic properties of R84F.

Enzymatic Properties of Arg73 Mutants. Upon substitution of the amino acid residues at position 73 of CYP105A1 (R73A, R73V, R73L, and R73F), the enzymatic activities of both the 25-hydroxylation of 1α(OH)D_3 and the 1α-hydroxylation of 25(OH)D_3 are increased, as shown in Table 3. This result is apparently similar to the case of Arg84 mutation. Of these mutants, both R73V and R73L showed an approximately 30 times higher k_{cat}/K_m value for the 25-hydroxylation of 1α(OH)D_3 than the wild type enzyme. The ratios of the 1α-hydroxylation to the 25-hydroxylation of the Arg73 mutants were 0.3−0.6. Even for the R73F mutant, the activity of the 25-hydroxylation is higher than that in the 1α-hydroxylation, showing that the effect of the Arg73 mutation is quite different from the Arg84 mutation.

Enzymatic Properties of Arg73/Arg84 Double Mutants. Based on the results of single mutation on Arg73 or Arg84, we constructed three double mutants (R73A/R84A, R73V/R84A, and R73V/R84F) to increase the activity in additive action. As expected, the three mutants exhibit higher 25-hydroxylation activity for 1α(OH)D_3 than any single mutant (Table 4 and Figure 5A). Double mutant R73V/R84A shows a 435-fold higher k_{cat}/K_m value for 25-hydroxylation than

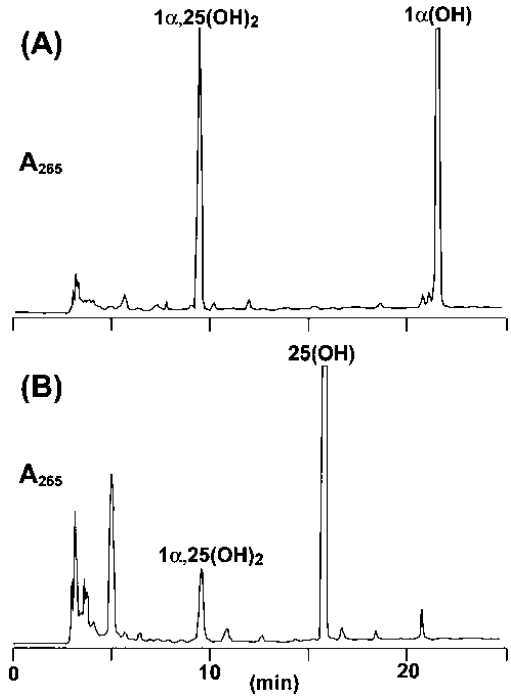

FIGURE 5: HPLC profiles of 1α(OH)D_3 (A) and 25(OH)D_3 (B) and their metabolites formed by the mutant R73V/R84A. After incubation with 10 μM substrate for 10 min (A) or 30 min (B), the reaction mixture was extracted and analyzed by HPLC as described under Materials and Methods.

the wild type. For the 1α-hydroxylation, the k_{cat}/K_m values of double mutants are also higher than those of any single mutant. The R73A/R84A mutant also shows a 319-fold higher k_{cat}/K_m for 25-hydroxylation. Figure 6 shows a crystal structure of R73A/R84A in complex with 1α,25$(OH)_2D_3$. Similar to the case of the R84A-1α,25$(OH)_2D_3$ complex, the 1α,25$(OH)_2D_3$ is bound to the transient binding site 12 Å from the iron atom along the I helix within the pocket. Although the difference in protein structure between the R84A-1α,25$(OH)_2D_3$ complex and the R73A/R84A−1α,25$(OH)_2D_3$ complex is very small (rmsd of 0.3 Å), the atomic position of 1α,25$(OH)_2D_3$ shows rmsd of 1.1 Å. In particular, conformation of the aliphatic side chain of 1α,25$(OH)_2D_3$ is considerably different, suggesting that a loss of the Arg73 side chain influences the position and conformation of 1α,25$(OH)_2D_3$ and possibly the substrates to enhance the activity.

We expected that the R73V/R84F mutant would show more 1α-hydroxylation activity than R84F. However, no further increase of 1α-hydroxylation activity was observed in R73V/R84F as compared with that of R84F, while 25-hydroxylation activity was remarkably enhanced.

The most interesting result in this study is the synergistic effect of substitutions of Arg84 and Arg73. Note that they locate in opposite sides of the substrate-binding site to sandwich the pocket as shown in Figure 2. It was proposed in the previous analysis that the substrate is initially bound to the observed binding site and then moves to a position that is suitable for metabolism (reaction site) (*9*). The amino acid residue at position 84 appears to have direct interaction with the compound in the transient binding site, and the indirect effect through the conformational changes of the other part of the active site pocket (i.e., the structure of the hydrophobic residues in the F helix and loop after the K helix) and the change in the gating mechanism of the B′ and F helices. On the other hand, amino acid residue at position 73 appears to affect the conformation of the compound during the reaction within the active site pocket including transient and reaction sites. Thus, the contributions of different mechanisms by two residues lead to the remarkable increase of activities.

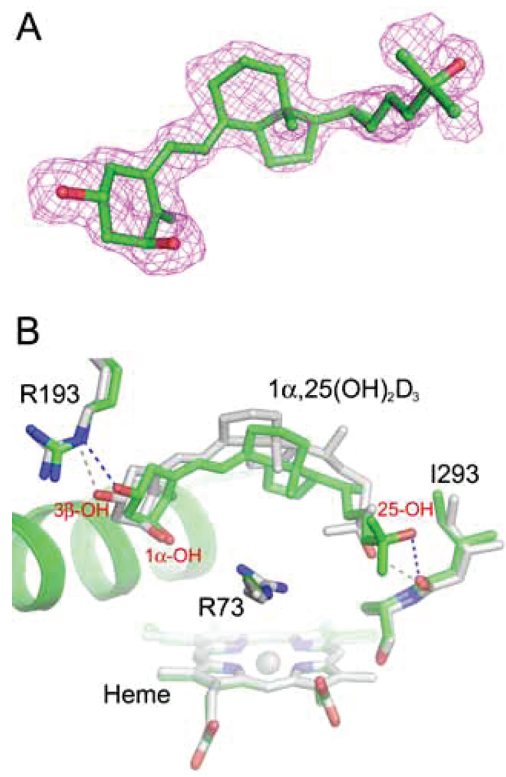

FIGURE 6: Compound 1α,25$(H)_2D_3$ in the active site of the R74A/R84A mutant of CYP105A1. (A) $F_o - F_c$ omit map (purple mesh). Electron density is contoured at 2.0σ. (B) Comparison of the R84A−1α,25$(H)_2D_3$ complex (PDB code 2ZBX, gray) and R73A/R84A−1α,25$(H)_2D_3$ complex (green). Nitrogen and oxygen atoms in the ball-and-stick model of both structures are shown in blue and red, respectively. Hydrogen bonds are shown as dotted lines between the donor and acceptor.

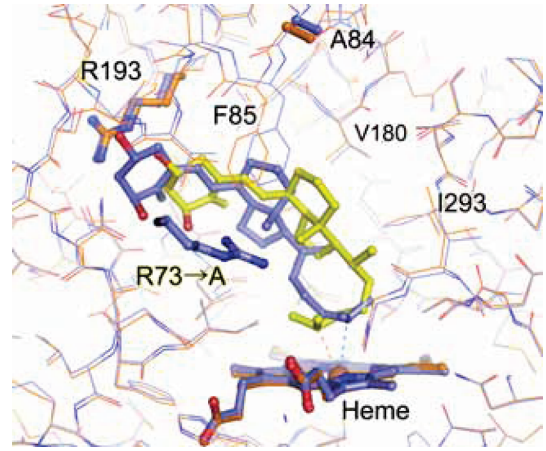

FIGURE 7: Comparison of docking models of the R84A mutant and R73A/R84A mutant. The R84A mutant with the docked 1α(OH)D_3 (light blue) is superimposed on the R73A/R84A mutant with docked 1αOH)D_3 (yellow). Nitrogen and oxygen atoms of enzymes and the compounds are shown in blue and red, respectively. Carbon atoms of R84A and R73A/R84A are shown in orange and light blue, respectively.

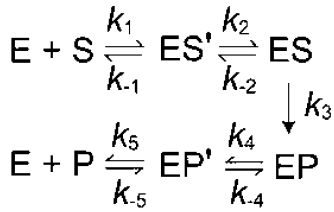

FIGURE 8: Putative kinetic scheme of wild type or mutant CYP105A1-dependent 25-hydroxylation of 1α(OH)D_3. E, S, and P represent wild type or mutant CYP105A1, 1α(OH)D_3, and 1α,25(OH)$_2D_3$, respectively. ES′ and EP′ represent the enzyme−substrate and enzyme−product complexes at the transient site as shown in Figure 6, respectively, while ES and EP represent the enzyme−substrate and enzyme−product complexes at the reaction site as shown in the docking model (Figure 7).

Relationships between Crystal Structure and Kinetics. In this section, we try to correlate crystal studies with kinetic studies. The crystal study demonstrated that 1α,25(OH)$_2D_3$ is preferentially bound to the transient sites of R84A and R73A/R84A. When the substrate 1α(OH)D_3 is also bound to the same site, enzyme reaction of the wild type and mutant CYP105A1 could be represented by a kinetic scheme shown in Figure 8, where ES′ and EP′ represent the enzyme−substrate and enzyme−product complexes at the transient site, respectively, while ES and EP represent the enzyme−substrate and enzyme−product complexes at the reaction site as shown in the docking model (Figure 7). When the concentration of the product [P] is much lower than the substrate [S], the initial rate v could be represented by the equation

$$v = k_{cat}^{app}[E]_0[S]/(K_m^{app} + [S]) \quad (1)$$

where

$$k_{cat}^{app} = k_2k_3k_4k_5/\{k_4k_5(k_2 + k_{-2} + k_3) + k_2k_3(k_4 + k_{-4} + k_5)\} \quad (2)$$

and

$$K_m^{app} = k_4k_5(k_{-1}k_2 + k_{-1}k_3 + k_2k_3)/\{k_1k_4k_5(k_2 + k_{-2} + k_3) + k_1k_2k_3(k_4 + k_{-4} + k_5)\} \quad (3)$$

As k_3 is considered to be much smaller than other rate constants, k_{-1}, k_2, k_{-2}, k_4, k_{-4}, and k_5, eqs 2 and 3 could be simplified as

$$k_{cat}^{app} = k_3/(1 + k_{-2}/k_2) \quad (4)$$

$$K_m^{app} = k_{-1}/\{k_1(1 + k_2/k_{-2})\} \quad (5)$$

Thus, the k_{cat} and K_m in Tables 3 and 4 correspond to k_{cat}^{app} and K_m^{app} in eqs 4 and 5, respectively.

We have obtained crystal structures of E (substrate-free enzyme) forms of the wild type, R84A, and R84F and EP′ forms of R84A and R73A/R84A. As mentioned above, comparison of E forms between the wild type and R84A revealed some change in the gating mechanism, which affects k_1, k_{-1}, k_5, and k_{-5}. When the release of the product is a rate-limiting step, increase of k_5 could enhance the catalytic activity as shown in eq 2. The fact that a crystal of EP′ of the wild type has not been obtained while EP′ of R84A has been successfully crystallized suggests that the structure of EP′ of R84A is significantly different from that of the wild type. As described in our previous report, position and conformation of 1α(OH)D_3 at the transient site of R84A appear similar to those of 1α,25(OH)$_2D_3$. Thus, ES′ of R84A is significantly different from that of the wild type, indicating the changes of k_1, k_{-1}, k_2, and k_{-2}. Similar K_m^{app} and remarkably larger k_{cat}^{app} values of R84A as compared with the wild type could be explained by the change of the k_2 and/or k_{-2} value. As mentioned above, the adaptability of the hydrophobic residues of the F helix (Leu180 and Val181) of R84A for substrate recognition increases the stability of the ES complex and would decrease k_{-2}/k_2 to increase k_{cat}^{app} as shown in eq 4. In addition, the change of position and conformation of the substrate in the ES complex could cause a large increase of k_3. Therefore, it is reasonable to assume that the mutation of Arg84 to Ala causes conformational change of ES′, ES, EP, and EP′ to affect most of the rate constants, and changes of k_2, k_{-2}, and k_3 may contribute to the remarkable increase of k_{cat}^{app}. The fact that the EP′ state of R73A/R84 including the position and conformation of 1α,25(OH)$_2D_3$ is different from that of R84A suggests that the ES′ state of R73A/R84 is also different from that of R84A. As shown in Figure 7, the position and conformation of the substrate in the ES state of R73A/R84 appears to be considerably different from those of R84A. These results strongly suggest that mutation at Arg73 significantly affects k_3 to increase k_{cat}^{app}. Thus, both mutations at positions 84 and 73 change many of the rate constants; however, it might be possible that the former mainly changes k_2 and/or k_{-2} due to the change of the ES′ state, and then the latter mainly changes k_3 due to the change of the ES state. If so, the synergistic effect of substitutions of Arg84 and Arg73 could be clearly explained by eqs 4 and 5. Another possibility is that distinct ES states among the wild type, R84A, and R73A/R84A to determine k_3 values are most critical. Because k_3 contains a series of P450 reactions including first electron transport, O_2 binding, second electron transport, O−O bond cleavage, hydrogen abstraction, rebound of OH group, and release of the product, further kinetic studies are needed to reveal the mechanism of the large increase of activity. Coupling efficiency between product formation and NADPH oxidation is another important point. Our preliminary results indicated that coupling efficiency of the mutants R84A and R73A/R84A is significantly improved from the wild type (data not shown), although those data are not sufficient to explain the large increase of activity.

Comparison of R73V/R84A with Native Vitamin D Hydroxylases CYP27A1 and CYP2R1. The activities of a wild type of CYP105A1 in metabolizing VD_3, 1α(OH)D_3, or 25(OH)D_3 are much lower than the physiologically important vitamin D hydroxylases such as CYP27A1, CYP2R1, and CYP27B1. However, the double mutant R73V/R84A shows higher k_{cat}/K_m values for both 1α(OH)D_3 25-hydroxylation activity and 25(OH)D_3 1α-hydroxylation activity than CYP27A1 (25-hydroxylation of 1α(OH)D_3: K_m = 6.9 μM, k_{cat} = 0.79 min^{-1}, k_{cat}/K_m = 0.11, 1α-hydroxylation of 25(OH)D_3: K_m =3.5 μM, k_{cat} =0.021 min^{-1}, k_{cat}/K_m = 0.006) (*19*). In particular, the k_{cat}/K_m value of the double mutant for 25(OH)D_3 1α-hydroxylation activity was 10 times higher than CYP27A1. In addition, R73V/R84A showed higher activity (turnover = 1.3 min^{-1}) than CYP2R1 ((turnover = 0.8 min^{-1}) at 10 μM of 1α(OH)D_3 (*20*)). These results strongly suggest that R73V/R84A has a fine structure as a vitamin D hydroxylase.

CONCLUSIONS

Very few chemical methods exist that directly hydroxylate aliphatic or aromatic C−H bonds, and most of them are not selective or of limited scope. Thus, biocatalysts such as P450s represent a promising alternative. Many published reports have been showing that actinomycete CYPs are practically useful for bioconversion and bioremediation (*21*−*24*). However, other applications have been limited by substrate specificity, low activity, and poor stability. To date, the most successful application of the P450 reaction on the industrial scale appears to be the bioconversion process for formation of pravastatin (an inhibitor of HMG-CoA reductase, an LDL-cholesterol-lowering drug) using a *Streptomyces* P450, CYP105A3 (*25, 26*). Protein engineering of CYPs has produced enzymes with altered substrate specificities, increased activity and stability. For example, our fusion technology between CYP and NADPH−CYP reductase remarkably increased the activity (*27*−*29*) and stability (*30*), and site-directed mutagenesis of CYP1A1 converted its function to a 2,3,7,8-TCDD-metabolizing enzyme (*31*). It is noted that our previous studies were performed without information on the tertiary structure of CYP. In this study, we used the information on the crystal structure of CYP105A1 in complex with 1α,25$(OH)_2D_3$ (*9*) to generate highly active vitamin D hydroxylase and confirmed the importance of tertiary structure to design highly active enzymes because we have obtained an excellent vitamin D hydroxylase in a short time.

In conclusion, we successfully enhanced the vitamin D_3 hydroxylation activity of CYP105A1 based on its tertiary structure. To our best knowledge, this is the first report showing a more than 400 times increase of CYP activity by site-directed mutagenesis. Structural analysis suggests that the altered properties of the enzyme are a result of the direct effect of substitution and indirect effect through the conformational differences in the B′ helix, F helix and loop after the K helix, which are coupled with an increase of hydrophobicity brought by mutations of Arg73 and Arg84 residues. The mutants are helpful for applying to the bioconversion process to produce 1α,25$(OH)_2D_3$ from vitamin D_3.

REFERENCES

1. Sakaki, T., Sawada, N., Nonaka, Y., Ohyama, Y., and Inouye, K. (1999) Metabolic studies using recombinant Escherichia coli cells producing rat mitochondrial CYP24: CYP24 can convert 1α,25-dihydroxyvitamin D_3 to calcitroic acid. *Eur. J. Biochem. 262*, 43–48.
2. Sasaki, J., Mikami, A., Mizoue, K., and Omura, S. (1991) Transformation of 25- and 1α-hydroxyvitamin D_3 to 1α,25-dihydroxyvitamin D_3 by using Streptomyces sp. strains. *Appl. Environ. Microbiol. 57*, 2841–2846.
3. Sasaki, J., Miyazaki, A., Saito, M., Adachi, T., Mizoue, K., Hanada, K., and Omura, S. (1992) Transformation of vitamin D_3 to 1α,25-dihydroxyvitamin D_3 via 25-hydroxyvitamin D_3 using Amycolata sp. strains. *Appl. Microbiol. Biotechnol. 38*, 152–157.
4. Kawauchi, H., Sasaki, J., Adachi, T., Hanada, K., Beppu, T., and Horinouchi, S. (1994) Cloning and nucleotide sequence of a bacterial cytochrome P-450VD25 gene encoding vitamin D_3 25-hydroxylase. *Biochim. Biophys. Acta 1219*, 179–183.
5. Sawada, N., Sakaki, T., Yoneda, S., Kusudo, T., Shinkyo, R., Ohta, M., and Inouye, K. (2004) Conversion of vitamin D_3 to 1α,25-dihydroxyvitamin D_3 by Streptomyces griseolus cytochrome P450SU-1. *Biochem. Biophys. Res. Commun. 320*, 156–164.
6. Omer, C. A., Lenstra, R., Litle, P. J., Dean, C., Tepperman, J. M., Leto, K. J., Romesser, J. A., and and O'Keefe, D. P. (1990) Genes for two herbicide-inducible cytochromes P-450 from Streptomyces griseolus. *J. Bacteriol. 172*, 3335–3345.
7. Winn, P. J., Lüdemann, S. K., Gauges, R., Lounnas, V., and Wade, R. C. (2002) Comparison of the dynamics of substrate access channels in three cytochrome P450s reveals different opening mechanisms and a novel functional role for a buried arginine. *Proc. Natl. Acad. Sci. U.S.A. 99*, 5361–5366.
8. Lee, D. S., Yamada, A., Sugimoto, H., Matsunaga, I., Ogura, H., Ichihara, K., Adachi, S., Park, S., and Shiro, Y. (2003) Substrate recognition and molecular mechanism of fatty acid hydroxylation by cytochrome P450 from Bacillus subtilis. *J. Biol. Chem. 278*, 9761–9767.
9. Sugimoto, H., Shinkyo, R., Hayashi, K., Yoneda, S., Yamada, M., Kamakura, M., Ikushiro, S., Shiro, Y., and Sakaki, T. (2008) Crystal structure of CYP105A1(P450SU-1) in complex with 1α,25-dihydroxyvitamin D_3. *Biochemistry 47*, 4017–4027.
10. Otwinowski, Z., and Minor, W. (1997) Proceeding of X-ray diffraction data collected in oscillation mode. *Methods Enzymol. 276*, 307–326.
11. Collaborative Computational Project, Number 4 (1994) The CCP4 suite: programs for protein crystallography, *Acta Crystallogr., Sect. D: Biol. Crystallogr. 50*, 760−763.
12. Emsley, P., and Cowtan, K. (2004) Coot: model-building tools for molecular graphics. *Acta Crystallogr., Sect. D: Biol. Crystallogr. 60*, 2126–2132.
13. Hiwatashi, A., Nishii, Y., and Ichikawa, Y. (1982) Purification of cytochrome P-450D1α (25-hydroxyvitamin D_3-1α-hydroxylase) of bovine kidney mitochondria. *Biochem. Biophys. Res. Commun. 105*, 320–327.
14. Morris, G. M., Goodsell, D. S., Halliday, R. S., Huey, R., Hart, W. E., Belew, R. K., and Olson, A. J. (1998) Automated docking using a Lamarckian genetic algorithm and an empirical binding free energy function. *J. Comput. Chem. 19*, 1639–1662.
15. Kleywegt, G. J., and Jones, T. A. (1994) Detection, delineation, measurement and display of cavities in macromolecular structures. *Acta Crystallogr., Sect. D: Biol. Crystallogr. 50*, 178–185.
16. Strushkevich, N., Usanov, S. A., Plotnikov, A. N., Jones, G., and Park, H. W. (2008) Structural analysis of CYP2R1 in complex with vitamin D_3. *J. Mol. Biol. 380*, 95–106.
17. Yamamoto, K., Uchida, E., Urushino, N., Sakaki, T., Kagawa, N., Sawada, N., Kamakura, M., Kato, S., Inouye, K., and Yamada, S. (2005) Identification of the amino acid residue of CYP27B1 responsible for binding of 25-hydroxyvitamin D_3 whose mutation causes vitamin D-dependent rickets type 1. *J. Biol. Chem. 280*, 30511–30516.
18. Hasemann, C. A., Kurumbail, R. G., Boddupalli, S. S., Peterson, J. A., and Deisenhofer, J. (1995) Structure and function of cytochromes P450: a comparative analysis of three crystal structures. *Structure 3*, 41–62.
19. Sawada, N., Sakaki, T., Ohta, M., and Inouye, K. (2000) Metabolism of vitamin D_3 by human CYP27A1. *Biochem. Biophys. Res. Commun. 273*, 977–984.
20. Shinkyo, R., Sakaki, T., Kamakura, M., Ohta, M., and Inouye, K. (2004) Metabolism of vitamin D by human microsomal CYP2R1. *Biochem. Biophys. Res. Commun. 324*, 451–457.
21. Healy, F. G., Krasnoff, S. B., Wach, M., Gibson, D. M., and Loria, R. (2002) Involvement of a cytochrome P450 monooxygenase in thaxtomin A biosynthesis by Streptomyces acidiscabies. *J. Bacteriol. 184*, 2019–2029.
22. Bruntner, C., Lauer, B., Schwarz, W., Mohrle, V., and Bormann, C. (1999) Molecular characterization of co-transcribed genes from Streptomyces tendae Tu901 involved in the biosynthesis of the peptidyl moiety of the peptidyl nucleoside antibiotic nikkomycin. *Mol. Gen. Genet. 262*, 102–114.
23. Lomovskaya, N., Otten, S. L., Doi-Katayama, Y., Fonstein, L., Liu, X. C., Takatsu, T., Inventi-Solari, A., Filippini, S., Torti, F., Colombo, A. L., and Hutchinson, C. R. (1999) Doxorubicin overproduction in Streptomyces peucetius: cloning and characterization of the dnrU ketoreductase and dnrV genes and the doxA cytochrome P-450 hydroxylase gene. *J. Bacteriol. 181*, 305–318.
24. Taylor, M., Lamb, D. C., Cannell, R., Dawson, M., and Kelly, S. L. (1999) Cytochrome P450105D1 (CYP105D1) from Streptomyces griseus: heterologous expression, activity, and activation effects of multiple xenobiotics. *Biochem. Biophys. Res. Commun. 263*, 838–842.
25. Matsuoka, T., Miyakoshi, S., Tanzawa, K., Nakahara, K., Hosobuchi, M., and Serizawa, N. (1989) Purification and characterization of cytochrome P-450sca from *Streptomyces carbophilus*. ML-236B (compactin) induces a cytochrome P-450sca in Streptomyces

carbophilus that hydroxylates ML-236B to pravastatin sodium (CS-514), a tissue-selective inhibitor of 3-hydroxy-3-methylglutaryl-coenzyme-A reductase. *Eur. J. Biochem. 184*, 707–713.
26. Serizawa, N., and Matsuoka, T. (1991) A two component-type cytochrome P-450 monooxygenase system in a prokaryote that catalyzes hydroxylation of ML-236B to pravastatin, a tissue-selective inhibitor of 3-hydroxy-3- methylglutaryl coenzyme A reductase. *Biochim. Biophys. Acta 1084*, 35–40.
27. Murakami, H., Yabusaki, Y., Sakaki, T., Shibata, M., and Ohkawa, H. (1987) A genetically engineered P450 Monooxygenase: Construction of functional fused enzyme between rat cytochrome P450c and NADPH-cytochrome P450 reductase. *DNA 6*, 189–197.
28. Sakaki, T., Kominami, S., Takemori, S., Ohkawa, H., Akiyoshi-Shibata, M., and Yabusaki, Y. (1994) Kinetic studies on a genetically engineered fused enzyme between rat cytochrome P4501A1 and yeast NADPH-P450 reductase. *Biochemistry 33*, 4933–4939.
29. Sakaki, T., Kominami, S., Hayashi, K., Akiyoshi-Shibata, M., and Yabusaki, Y. (1996) Molecular engineering study on electron transfer from NADPH-P450 reductase to rat mitochondrial P450c27 in yeast microsomes. *J. Biol. Chem. 271*, 26209–26213.
30. Sakaki, T., Shibata, M., Yabusaki, Y., Murakami, H., and Ohkawa, H. (1990) Expression of bovine cytochrome P450c21 and its fused enzymes with yeast NADPH-cytochrome P450 reductase in Saccharomyces cerevisiae. *DNA Cell Biol. 9*, 603–614.
31. Shinkyo, R., Sakaki, T., Takita, T., Ohta, M., and Inouye, K. (2003) Generation of 2,3,7,8-TCDD-metabolizing enzyme by modifying rat CYP1A1 through site-directed mutagenesis. *Biochem. Biophys. Res. Commun. 303*, 511–517.

BI801222D